Journal of ELECTRONIC MATERIALS, Vol. 49, No. 5, 2020
https://doi.org/10.1007/s11664-020-08029-6
© 2020 The Minerals, Metals & Materials Society

Electronic, Elastic, Vibrational and Thermodynamic Properties of HfIrX (X = As, Sb and Bi) Compounds: Insights from DFT-Based Computer Simulation

NİHAT ARIKAN,[1,5] GÖKÇEN DİKİCİ YILDIZ,[2] YASİN GÖKTÜRK YILDIZ,[3] and AHMET İYİGÖR[4]

1.—Department of Mathematics and Science, Education Faculty, Ahi Evran University, 40100 Kırşehir, Turkey. 2.—Department of Physics, Faculty of Arts and Sciences, Kırıkkale University, 71450 Kırıkkale, Turkey. 3.—Department of Electronics and Automation, Kırıkkale University, 71480 Kırıkkale, Turkey. 4.—Department of Machinery and Metal Technology, Ahi Evran University, 40100 Kırşehir, Turkey. 5.—e-mail: nihat.arikan@hotmail.com

Ab-initio calculations were performed to reveal and thoroughly understand the structural, electronic, elastic, thermodynamic and vibrational properties of HfIrX (X = As, Sb and Bi) compounds in the $C1_b$ phase. Basic physical characteristics, such as bulk modulus, pressure derivative of bulk modulus, anisotropy factor, shear modulus, Poisson's ratio, Cauchy pressure, elastic constants and Young's modulus were obtained and some of them were compared with those in the literature. Electronic band structure, the density of states and phonon dispersion curves were obtained and compared with current theoretical calculations. It was concluded according to current band structure calculations that the HfIrAs and HfIrBi compounds showed semimetal characteristics, while the HfIrSb compound behaves as a semiconductor. It was determined based on phonon calculations that all three compounds were dynamically stable. Various thermodynamic properties, such as heat capacity, thermal expansion coefficient values and Grüneisen parameter were calculated under constant volume and constant pressure by using Gibbs2 code within the Quasi-harmonic approach, and these results are discussed.

Key words: *Ab-initio*, DFT, elastic constant, electronic structure, phonon, thermodynamic

INTRODUCTION

Half-Heusler (ABX) compounds consist of a rare earth or transition metal (A), a transition metal (B) and the main group element (X). These ABX compounds have $C1_b$ structure (space group F-43 m) with three Wyckoff positions, 4a (0, 0, 0), 4b (½, ½, ½) and 4c (¼, ¼, ¼). Many of the $C1_b$-structured compounds are found in the half-metallic ferromagnetic class.[1,2] The ferromagnetic behaviour of the half-Heusler compounds was first observed by de Groot et al.[3] In recent years, several attempts have been made to understand the structural, thermoelectric, elastic, magnetic and optical properties of half-Heusler alloy systems. Recently, half-Heusler compounds have attracted researchers' attention in the fields of superconductivity and spintronics because of their high-temperature stability; for this reason, many researchers are focused on thermoelectric compounds.[4,5] Besides experimental[6–11] examination of these compounds related their thermoelectric properties, theoretical research[12–26] is devoted to the analyses of structural, elastic, magnetic and optical properties of these materials. Hafnium and hafnium-based compounds can be used in nuclear power plants because of their high corrosion resistance and high neutron cross sections. They are primarily used as nuclear

(Received August 26, 2019; accepted February 17, 2020; published online February 27, 2020)

control rods, nozzles for plasma arc metal cutting and high-temperature ceramics.[27–30] Benallou et al.[17] studied the structural stability and thermoelectric properties of ZrIrM (M = As, Bi, and Sb) compounds by using a density functional theory (DFT) based method. Li et al.[27] reported the structural, electronic and elastic properties of HfM (M = Os, Ir, and Pt) using DFT with generalized gradient approximation (GGA) and local density approximation (LDA) methods.

Studies on the structural analysis, optical, elastic and thermoelectric properties of HfIrM (M = As, Sb and Bi) compounds are available in the literature.[31–36] For example, Chibani et al.[31] theoretically studied the thermoelectric and optoelectronic properties of HfIrM (M = As, Sb and Bi) using a full-potential linearized augmented plane wave (FP-LAPW) method. Their work provides a detailed view of the optoelectronic, thermoelectric and structural calculation of HfIrM (M = As, Sb and Bi) compounds. On the other hand, Gautier et al.[32] studied the half-Heusler materials with 18 electrons of ABX ternary compounds and theoretical estimation of some physical properties of HfIrX (X = As, Sb, and Bi) by using the hybrid functional (HSE06) with spin-orbit coupling (SOC). We found no studies in the literature investigating similar physical properties of HfIrSn materials. Wang and Wei[33] studied the lattice constant, atoms substitutions, and tunable topological phases changes in the half-Heusler compounds HfIrM (M = As, Sb, and Bi). They reported that at the equilibrium cubic crystal structure and excluding SOC, HfIrAs and HfIrBi are nontrivially topological semimetals, while HfIrSb is a trivial topological insulator. For the microscopic understanding of lattice dynamics, full phonon spectra play an important role in stability and determining various basic solid-state properties such as thermal expansion, electron–phonon interaction, heat conduction and phase transitions, and can be very useful for investigating these properties. Previous research efforts are mainly focused on the structural and electronic properties of these compounds, while the dynamical properties have been relatively less studied in the literature. None of the prior studies explore the second-order elastic constants and the related elastic properties of those materials. Simulation modelling of materials based on accurate *ab-initio* methods has been an important problem in estimating the properties of materials, and provides an important tool for discovering some properties that have not yet been experimentally investigated or are difficult to measure experimentally. Therefore, we carried out plane-wave pseudopotential *ab-initio* calculations of many physical properties of HfIrX (X = As, Sb, Bi). The computed results include optimized structural parameters, elastic constants and their respective properties, electronic band structures and corresponding partial density of state, phonon dispersion curves and corresponding projected density of state, and various thermodynamic properties.

METHOD

Ab-initio calculations were carried out using the Quantum-ESPRESSO program package[37,38] to study the structural, electronic, elastic and vibrational properties of HfIrX (X = As, Bi and Sb) compounds. The electron–ion interactiowasen calculated by GGA using the scheme of Perdew–Burke–Ernzerhof (PBE)[39] exchange–correlation potential. The cut-off values for the single particle wave functions and electronic charge density were evaluated to be 40 and 400 Ry, respectively. Integration up to the Fermi surface was performed using the Methfessel–Paxton[40] smearing technique with the smearing parameter σ = 0.02 Ry. Having obtained self-consistent solutions of the Kohn–Sham equations, the lattice-dynamical properties of HfIrX (X = As, Bi and Sb) were investigated within the framework of self-consistent density functional perturbation theory.[41,42] In order to obtain full phonon dispersions and density of states, eight dynamical matrices were computed for a $4 \times 4 \times 4$ q-point mesh in the irreducible Brillouin zone. These dynamical matrices can be evaluated by means of a Fourier deconvolution. The thermodynamic properties have been calculated under constant volume and constant pressure by using Gibbs2 code with the quasi-harmonic approach.

The *ab-initio* pseudopotential method allows total energy calculations for arbitrary crystal structures. This method helped us to apply a small amount of strain to the equilibrium lattice to find the change in total energy and then to derive elastic constants with the help of this information. Elastic constants are defined as a function of deformation parameter (δ) proportional to the second-order coefficient within a polynomial harmony of total energy.

There are three independent elastic constants for a cubic lattice: C_{11}, C_{12} and C_{44}. Thus, three equations are necessary to determine these constants. Equation (1) calculates bulk modulus (B), which depends on the values of C_{11} and C_{12}[43,44]

$$B = (C_{11} + 2C_{12})/3. \tag{1}$$

Equation (2) (tetragonal shear modulus) includes volume-conservation tetragonal strain to determine $C_{11} - C_{12}$

$$\bar{\varepsilon} = \begin{pmatrix} \delta & 0 & 0 \\ 0 & \delta & 0 \\ 0 & 0 & (1+\delta)^{-2}-1 \end{pmatrix}. \tag{2}$$

This strain provides energy change, $\Delta E = 3V_o (C_{11} - C_{12})\delta^2 + O\ [\delta^3]$. Equation (3) includes a strain volume-conservation base-centered orthorhombic strain tensor

$$\bar{\varepsilon} = \begin{pmatrix} \delta & \delta/2 & 0 \\ \delta/2 & 0 & 0 \\ 0 & 0 & \frac{\delta^2}{(4-\delta)^2} \end{pmatrix}. \quad (3)$$

This strain provides energy change, $\Delta E = 1/2C_{44}V_o\delta^2 + O\ [\delta^4]$. This energy alteration directly gives a C_{44} value, and C_{11} and C_{12} values are calculated by combining the tetragonal shear modulus associated with the bulk modulus in Eq. 1. Elastic constants of HfIrX compounds in the $C1_b$ phase are examined as a function of hydrostatic pressure by calculating bulk modulus (B) and two different shear moduli ($C' = (C_{11} - C_{12})/2$ and C_{44}) at various volumes. Detailed calculations of the elastic constant calculation method were reported in previous studies.[45,46] For cubic structure, the shear modulus G is defined from Voigt (G_v) and Reuss (G_R) modules as shown in Eq. 4:

$$G = \frac{G_V + G_R}{2}, \quad G_V = \frac{C_{11} - C_{12} + 3C_{44}}{5} \text{ and } G_R = \frac{5C_{44}(C_{11} - C_{12})}{4C_{44} + 3(C_{11} - C_{12})}. \quad (4)$$

The anisotropy factor (A) is calculated by using Eq. 5:

$$A = 2C_{44}/(C_{11} - C_{12}). \quad (5)$$

Young's modulus is calculated as shown in Eq. 6:

$$E = \frac{9BG}{3G + B}. \quad (6)$$

Poisson's ratio is expressed in Eq. 7:

$$v = \frac{(3B - 2G)}{2(3B + G)}. \quad (7)$$

To obtain some important thermodynamic values, such as Debye temperature and heat capacity, the calculations are carried out with a quasi-harmonic approach by using Gibbs2 Code as described in Ref. 47.

Helmholtz free energy is calculated as follows in Eq. 8:

$$U = nk_bT\left[\frac{9}{8}\frac{\theta_D}{T} + 3\ln\left(1 - e^{-\frac{\theta_D}{T}}\right) - D\left(\frac{\theta_D}{T}\right)\right], \quad (8)$$

where $D(\frac{\theta_D}{T})$ is the Debye function expressed in Eq. 9:

$$\left(\frac{\theta_D}{T}\right) = 3\left(\frac{T}{\theta_D}\right)\int_0^{\theta_D}\frac{z^2 dz}{e^z - 1} \quad (9)$$

RESULTS AND DISCUSSION

HfIrX (X = As, Sb and Bi) compounds considered in this study were investigated in the $C1_b$ phase. The compounds in this phase crystallize in a cubic structure with the $Fm\bar{3}m$ (#225) space group, as shown in Fig. 1. Hf atoms at the center of the unit cell are positioned at (0.5, 0.5, 0.5), Ir atoms are positioned at (0.25, 0.25, 0.25) and the third atoms (X = As, Sb, and Bi) are found in the corners (0, 0, 0). In the first stethe p, equilibrium lattice constant was determined by minimizing total energy based on different values of lattice constants. Calculated total energies were fitted for the Murnaghan equation of state. Basic state properties such as equilibrium lattice constants (a_0), bulk modulus (B) and pressure derivative of bulk modulus (B') were calculated as presented in Table I. It was seen that calculated structural parameters were reasonably in accordance with previous calculations.[31–33,35,36] As shown in Table I, The HfIrAs compound has the largest bulk modulus value, thus it can be compressed more than the other two compounds. In the periodical table, moving from the top to the bottom in Group 5A which includes elements As and Bi, the bulk modulus value gradually decreases. This indicates that the compressibility of an atom decreases as its atomic number increases.

The response of a crystal to applied external forces is determined by elastic constants; therefore, elastic constants provide significant information about the mechanical properties of solid materials. For example, structural stability, anisotropic characteristic and bonding properties of materials can be determined by elastic constants. HfIrX compounds have cubic structure, so elastic properties of these compounds are defined by three independent elastic constants C_{11}, C_{12} and C_{44}. The elastic constants given in Table I have positive values. For these values of elastic constants, the Born elastic stability criteria given in Eqn. 10 are met.[48]

$$C_{11} > 0, \quad C_{44} > 0, \quad C_{12} < B < C_{11}, \quad C_{11} - C_{12} > 0, \quad C_{11} + 2C_{12} > 0. \quad (10)$$

Anisotropy measures the structural stability of a material and transfer probability of microcracks.[49,50] When a crystal is isotropic, its anisotropy index should be equal to 1. The deviation value of the index from 1 corresponds to the elastic anisotropy degree of the crystal. For the compounds examined, the values of A deviated from 1, so the three compounds are elastically anisotropic. This means that when all three materials are grown, they have a high possibility of including microcracks or structural defects.

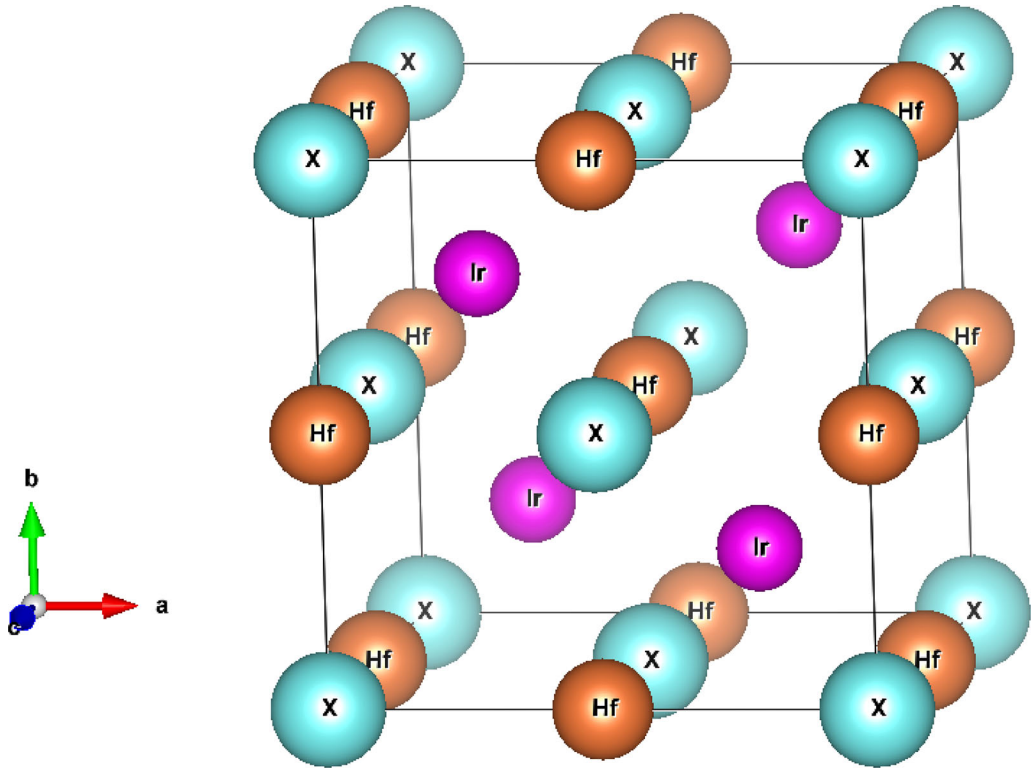

Fig. 1. Crystal structure of HfIrX (X = As, Sb and Bi) compounds in the $C1_b$ phase.

Table I. Lattice constant (Å), bulk modulus (GPa), pressure derivative of bulk modulus and elastic constant (GPa) values of HfIrX (X = As, Sb and Bi) compounds in the $C1_b$ phase

Materials	References	a (Å)	B (GPa)	B'	C_{11} (GPa)	C_{12} (GPa)	C_{44} (GPa)	CP = ($C_{12} - C_{44}$)
HfIrAs	Without SOC	6.138	156.200	4.92	222.418	129.837	94.199	35.638
	With SOC	6.123	160.9	4.65	227.221	129.593	68.336	61.257
	FP-LAPW[31]	6.090	176.071	4.22				
	VASP[32]	6.159						
	STATE[33]	6.160						
HfIrSb	Without SOC	6.332	150.500	4.00	243.158	113.701	95.445	18.256
	With SOC	6.324	166.7	3.22	246.629	114.375	72.870	41.505
	FP-LAPW[31]	6.277	171.722	4.78				
	Exp[32]	6.270						
	VASP[32]	6.345						
	STATE[33]	6.329						
	VASP[35]	6.340						
	VASP[36]	6.180						
HfIrBi	Without SOC	6.448	143.100	3.81	216.824	101.455	76.071	25.384
	With SOC	6.451	135.6	4.77	208.321	94.251	52.163	42.088
	FP-LAPW[31]	6.381	153.247	4.20				
	VASP[32]	6.476						
	STATE[33]	6.490						

Brittleness or ductility of a material is measured by using various parameters. Cauchy pressure (CP) is obtained based on two elastic constants (C_{12} and C_{44}) by using Eq. 11, developed by Pettifor in 1992.[51]

$$\mathrm{CP} = C_{12} - C_{44}. \tag{11}$$

CP values calculated in our study are presented in Table I, and positive CP values of HfIrX compounds validate their ductility. When compared with the values in Table II, the highest CP value was found in HfIrAs, which is thus the most ductile material. Another important parameter measuring

the ductility and brittleness of a material is the bulk to shear modulus (B/G) ratio proposed by Pugh.[52] If the B/G ratio is higher than 1.75, the material is ductile; otherwise, it is brittle. HfIrX compounds have B/G ratio values higher than 1.75, which proves that they are ductile. The third parameter measuring ductility and brittleness of materials is Poisson's ratio (v). If a material's v value is higher than 0.26, it is ductile; otherwise, it is brittle. Our calculated v value of HfIrX compounds is higher than 0.26, as shown in Table II. This result proves, again, that the HfIrAs compound is the most ductile. The rigidity of materials is defined by shear modulus (G). B, G, GV and GR values obtained for HfIrX compounds are shown in Table II. Another well-known parameter related to the rigidity of materials is Young's modulus (E). A higher E value for a material indicates that it is more rigid. It should be considered that the covalent property of a material increases with increasing E; thus, this affects the material's ductility. Calculated E values have great importance in terms of rigidity of these materials. When a comparison is made for the three studied compounds, the HfIrSb compound is the most rigid material (E = 208.815 GPa), while the HfIrBi compound has the lowest rigidity (E = 175.764 GPa). When the calculations with spin–orbit coupling (SOC) are compared to the calculations without SOC, it can be said that, although there is no significant change in bulk modulus for all three compounds, compressibility increases due to the decrease in shear modulus. Young's modulus, which is also an expression of hardness, shows a decrease. This indicates a decrease in the hardness of the materials. In addition, the reduction in C_{44}, which indicates resistance to shear deformation, supports these conditions. Another parameter based on the calculation of elastic constants is microhardness (H). Hardness can be studied by calculating the microhardness (H) parameter given in Eq. 12:

$$H = \frac{(1-2\sigma)E}{6(1+\sigma)}. \qquad (12)$$

Calculated H values are 9.119, 9.537 and 12.09 GPa for HfIrAs, HfIrSb and HfIrBi compounds, respectively. It is seen based on these values that H(HfIrBi) > H(HfIrSb) > H(HfIrAs).

Electronic band structure of HfIrX compounds was calculated across highly symmetric directions in the Brillouin zone by using GGA; results are presented in Fig. 2. As can be seen from Fig. 2, because the maximum of the valence band and the minimum of the conduction band are zero-clearance at the Γ symmetry point for the HfIrAs and HfIrBi compounds, these materials are semi-metals. HfIrSb is a semiconductor with an approximately 0.82 eV band gap value at the Γ point. When calculated electronic band structures of HfIrX compounds are examined comparatively, the results accord with those reported in previous studies.[31–36] Considering SOC, the SOC electronic band structure of all three materials splits up at the bands around the Fermi level. This indicates that HfIrSb is a semiconductor while HfIrAs and HfIrBi are semi-metals. When electronic band structures of the HfIrAs (HfIrBi) and HfIrSb compounds are examined, it is seen that there is band inversion among them. As described by Zunger et al.,[32] the band inversion causes topological phase transition. The band inversion depends on hybridization strength and spin–orbit coupling size.[53] There is a strong hybridization between s-orbitals of HfIrSb, which leads to a wide energy gap between bonding and anti-bonding. All these results, with and without SOC calculations, are in good agreement with Ref. 31. For HfIrSb, the band gap decreased to 0.70 eV. To better understand the electronic band spectra of these compounds, it is meaningful to draw their total and projected density of states (DOS). Accordingly, Fig. 3 shows total and projected DOS values. In the electronic band structure of the three compounds, the main contribution to DOS is provided by d orbitals of the Hf and Ir elements. It can be seen from total and projected DOS of HfIrX compounds given in Fig. 3 that two peaks are distributed above and below the Fermi level. The contributions to the peak above Fermi level are due to Hf 5d, As 4p, Sb 6p and Bi 6p orbitals for HfIrAs, HfIrSb and HfIrBi compounds. In electronic cases below the Fermi level, Ir 5d, Hf 5d and Ir 6p cases are dominant, while As 4p (Sb 6p and Bi 6p) cases make the secondary contribution. The main contributions to DOS at the Fermi level are mainly due to

Table II. Bulk modulus (GPa), Debye temperature (K), shear modulus (GPa), Cauchy pressure, B/G ratio, anisotropy, Young's modulus (GPa) and Poisson's ratio values of HfIrX (X = As, Sb and Bi) compounds in $C1_b$ phase

Materials	References	B (GPa)	Θ_D (K)	G (GPa)	G_V (GPa)	G_R (GPa)	B/G	A	E (GPA)	v
HfIrAs	Without SOC	160.698	277.57	70.827	75.035	66.619	2.268	2.034	185.264	0.307
	With SOC	162.136	268.38	59.336	60.546	58.925	2.732	1.399	159.603	0.34
HfIrSb	Without SOC	156.854	265.04	81.688	83.158	80.218	1.920	1.474	208.815	0.278
	With SOC	158.460	280.464	70.093	70.173	70.014	2.260	1.101	183.259	0.31
HfIrBi	Without SOC	139.912	229.06	68.092	68.716	67.469	2.054	1.318	175.764	0.278
	With SOC	132.274	229.67	54.060	54.112	54.008	2.446	0.914	142.734	0.32

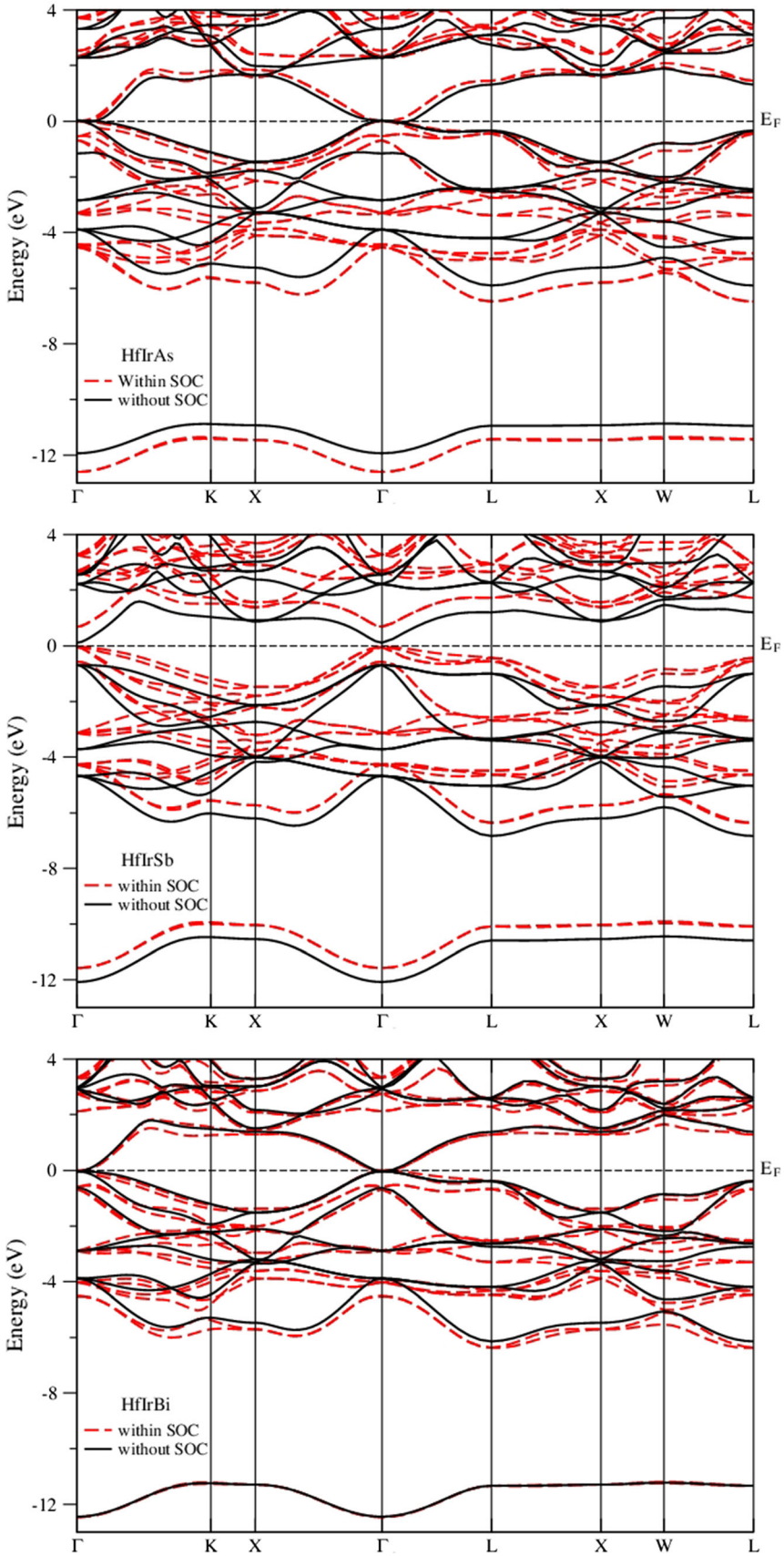

Fig. 2. Electronic band structures of HfIrX (X = As, Sb and Bi) compounds with and without SOC in the $C1_b$ phase.

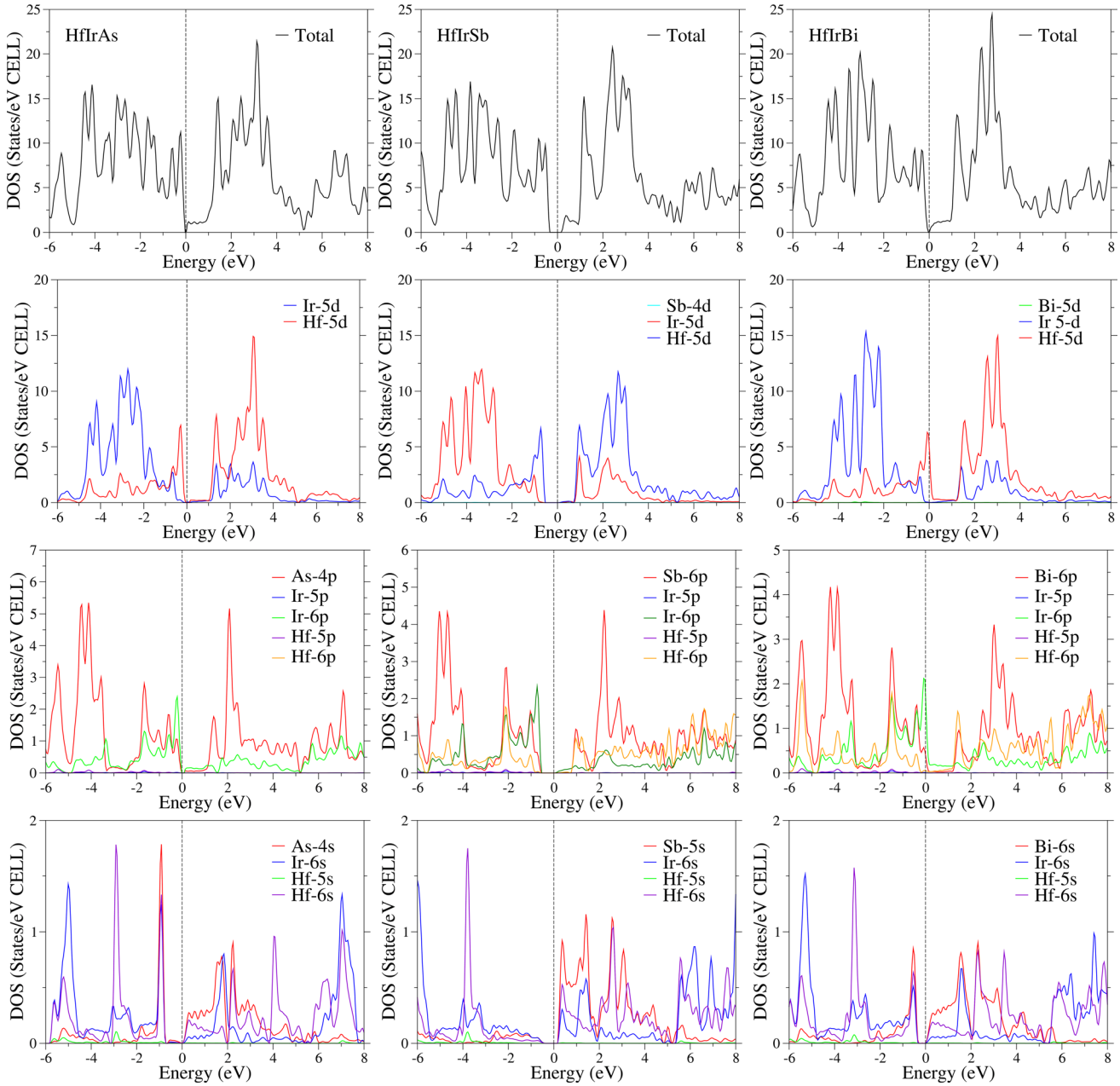

Fig. 3. Projected density of states of HfIrX (X = As, Sb and Bi) compounds in the $C1_b$ phase.

Hf 5*d* orbitals and Ir 6*p* orbitals for HfIrAs and HfIrBi compounds.

Figure 4 shows the phonon spectrum, total and projected DOS of HfIrX compounds in the $C1_b$ phase. Phonon characteristics of HfIrX compounds were calculated (by Fm3m (225) space group symmetry) in the $C1_b$ phase using GGA. Because these compounds have three atoms in their unit cells in the $C1_b$ phase, their phonon dispersion curves include three acoustic and six optical branches. For the three materials, the difference between acoustic and optical branches is not necessary to form a vacancy. Because of symmetry, the number of different phonon branches in the $C1_b$ phase decreases across main symmetry directions, except for Γ–*K* direction. As can be seen from Fig. 4, all phonon branches of the three compounds have positive frequencies, which indicate dynamic stability in the $C1_b$ phase. The highest optical branches for HfIrSb are separated from the remaining phonon branches with a 0.11 THz frequency. For HfIrAs and HfIrBi, differentiation between acoustic and optical branches is not necessary to form a vacancy. The highest frequency values were found to be 5.25 THz, 6.07 THz and 5.35 THz for total DOS of HfIrX (X = As, Sb and Bi) compounds, respectively. The frequencies of optical phonon modes of HfIrX compounds were calculated; they

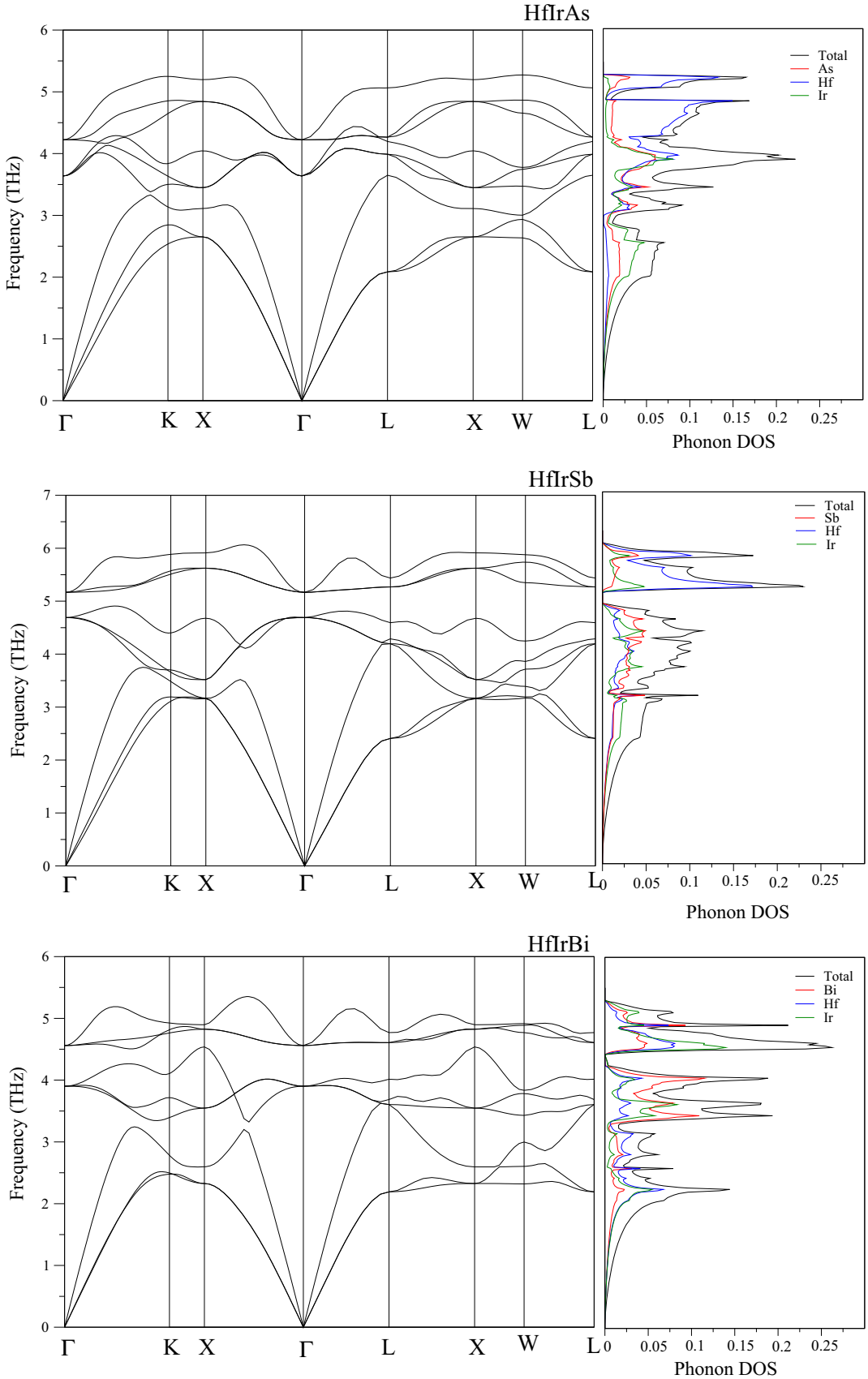

Fig. 4. Phonon distribution curves of HfIrX (X = As, Sb and Bi) compounds in the $C1_b$ phase across some high symmetry directions.

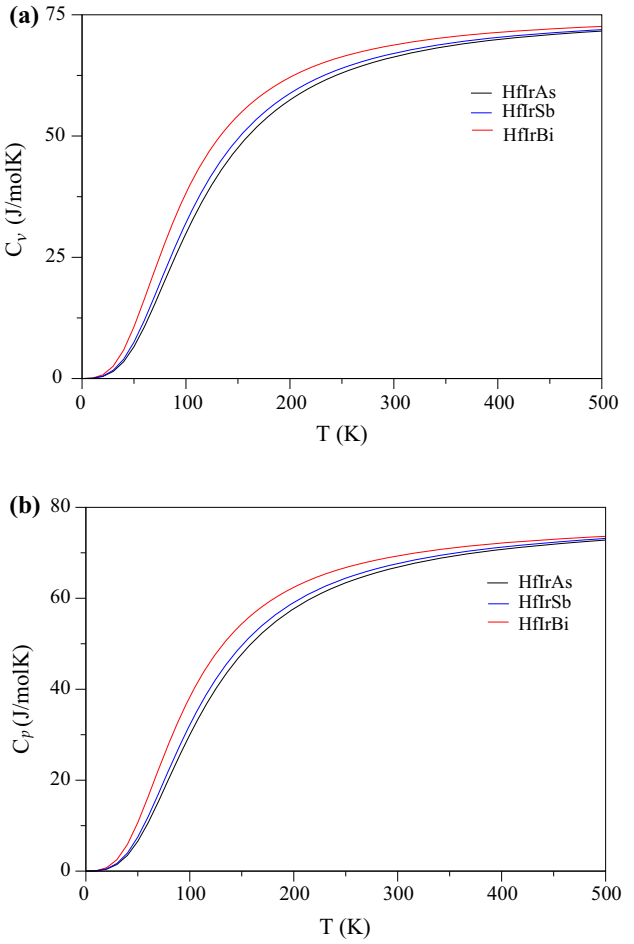

Fig. 5. Temperature dependence of specific heat capacity at (a) constant volume and (b) constant pressure.

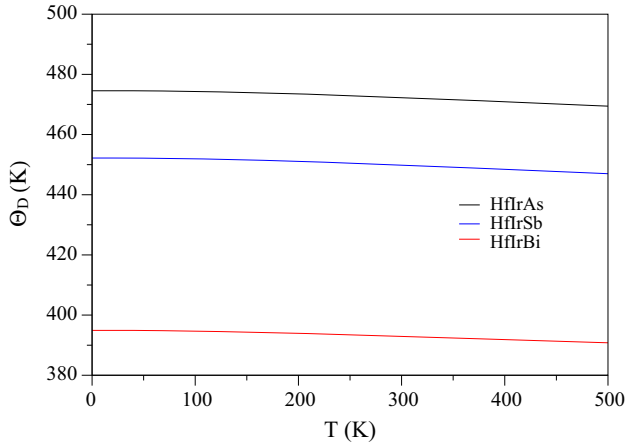

Fig. 6. Changes of HfIrX (X = As, Sb and Bi) compounds at Debye temperature.

were determined to be 3.63 and 4.23 THz for HfIrAs, 4.69 THz and 5.16 THz for HfIrSb, and 3.89 THz and 4.56 THz for HfIrBi. Experimental data in the literature compare to the calculated phonon frequencies of materials considered in this study.

Thermodynamics is a key constituent of physics and material science; therefore, some thermodynamic parameters of HfIrX compounds, such as constant volume specific heat capacity (C_V), Debye temperature, thermal expansion coefficient and Grüneisen parameter, were calculated from energy-volume data under temperature change by using Gibbs2 code with the quasi-harmonic approach. Thermodynamic properties of HfIrX were monitored at a temperature range between 0 and 500 K, which is below the melting point of all three compounds. Figure 5a, b shows temperature dependency of constant-volume heat capacity (C_V) and constant-pressure heat capacity (C_P), respectively. It can be seen from the figure that the curves of C_V and C_P are very similar to each other. For a temperature range between 0 and 200 K, C_V and C_P values rapidly increase. When the temperature is higher than 200 K, the anharmonic effect on C_V is suppressed, and C_V gradually increases with increasing temperature to approach a constant value called the Dulong–Pettit limit,[54] which is common for all solids at high temperatures. On the other hand, C_P monotonically increases with increasing temperature.

Debye temperature (Θ_D) is defined as the highest temperature of a normal vibrational mode of a crystal. This temperature is one of the most valuable physical parameters for providing information about various characteristics, such as phonons, thermal expansion, thermal conductivity, heat capacity and lattice enthalpy. Figure 6 shows the change in Debye temperature (Θ_D) at different temperatures. For the three materials, it is clearly seen that Debye temperature has a slow downward trend between 0 and 500 K. Thus, the slow change in Θ_D with temperature reflects the small effect of temperature on Θ_D. Vibration frequency is proportional to the square root of hardness in the harmonic approach. The hardness of solids can be estimated from the Debye temperature and is called Debye hardness. Maximum phonon frequency of the frequency spectrum is proportional to the square root of hardness in the harmonic approach. Both θ_D and maximum phonon frequency can be used in determining Debye hardness of solids as an estimation tool. Accordingly, as can be seen from Fig. 6, HfIrAs has the highest Debye hardness while HfIrBi has the lowest Debye hardness. The degree of expansion of a material upon heating is usually defined by the thermal expansion coefficient (α). When different materials are heated, they show different expansion trends. For small temperature ranges, thermal expansion coefficients are proportional to temperature change. Change in thermal expansion coefficients of HfIrX compounds is shown as a function of temperature in Fig. 7. For $T < 200$ K, the thermal expansion coefficient rapidly increases with increasing temperature in

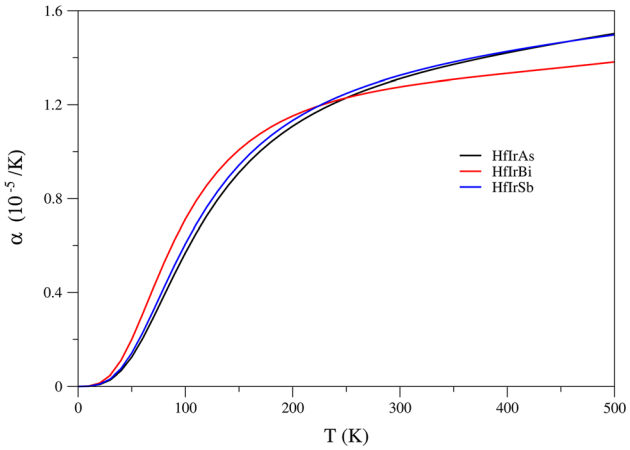

Fig. 7. Thermal expansion coefficient changes of HfIrX (X = As, Sb and Bi) compounds with respect to temperature.

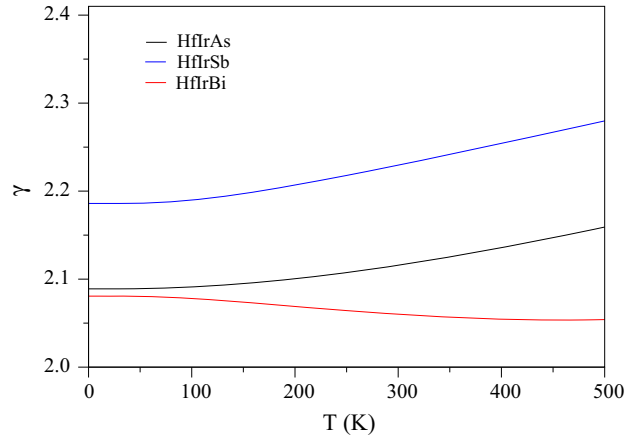

Fig. 8. Grüneisen parameter of HfIrX (X = As, Sb and Bi) compounds based on temperature.

all compounds, increasing by T^3 at lower temperatures. At higher temperatures, the increase in α becomes smoother with increasing temperature and gradually approaches a linear behavior. Grüneisen parameter (γ) explains the change in vibration properties of a crystal lattice due to volume increases or decreases caused by temperature change. The change in the Grüneisen parameter as a function of temperature is shown in Fig. 8. Grüneisen parameter of HfIrAs and HfIrSb compounds increases slowly with temperature. For HfIrBi, an increase is observed after a slow decrease up to 500 K.

CONCLUSION

Structural, electronic, elastic, thermodynamic and phonon properties of HfIrX compounds were studied by using GGA within the frame of *ab-initio* DFT. Second-order elastic constants and related elastic properties were computed and evaluated for the first time. Data obtained from equilibrium lattice constants, elastic constants, bulk modulus, shear modulus and Young's modulus validated that all three compounds were elastically and structurally stable. Cauchy pressure, anisotropy, Pugh ratio and Poisson's ratio revealed that three compounds were ductile. Calculated elastic constant values showed mechanical stability in all three materials because they satisfied the Bohr stability principle. It was observed from electronic structure calculations that the HfIrAs and HfIrBi compounds presented semi-metal characteristic because their conduction bands reached minima and their valence bands reached maxima at the Γ point, while the HfIrSb compound was a semiconductor with a 0.82 eV band gap, which is in accordance with the literature. For HfIrX (X = As, Sb and Bi) compounds in $C1_b$ phase, phonon dispersion curves and corresponding total and projected DOS were calculated with density functional perturbation theory. Because a negative value was not observed in calculated phonon distribution curves, it was found that all three materials were dynamically stable. As a result of thermodynamic research, various thermodynamic properties such as heat capacity, thermal expansion coefficient and Grüneisen parameter were obtained for HfIrX compounds by using a quasi-harmonic approach.

REFERENCES

1. M. Ahmad, K. Naeemullah, G. Murtaza, R. Khenata, S. Bin Omran, A. Bouhemadoue, *J. Magn. Magn. Mater.* 377, 204 (2015).
2. S. Chibani, O. Arbouche, M. Zemouli, K. Amara, Y. Benallou, Y. Azzaz, B. Belgoumène, A. Bentayeb, M. Ameri, *J. Electron. Mater.* 47, 196 (2018).
3. R.A. De Groot, F.M. Mueller, P.G. Van Engen, K.H.J. Buschow, *Phys. Rev. Lett.* 50, 2024 (1983).
4. G.S. Nolas, J. Poon, M. Kanatzidis, *MRS Bull.* 31, 199 (2006).
5. H. Hohl, A.P. Ramirez, C. Goldmann, G. Ernst, B. Wlfing, E. Bucher, *J. Condens. Matter. Phys.* 11, 1697 (1999).
6. G. Li, K. Kurosaki, Y. Ohishi, H. Muta, S. Yamanaka, *Jpn. J. Appl. Phys.* 52, 041804 (2013).
7. S. Populoh, M.H. Aguirre, O.C. Brunko, K. Galazka, Y. Lu, A. Weidenkaff, *Scr. Mater.* 66, 1073 (2012).
8. G. Joshi, X. Yan, H. Wang, W. Li, G. Chen, Z. Ren, *Adv. Energy Mater.* 1, 643 (2011).
9. C. Uher, J. Yang, S. Hu, D.T. Morelli, G.P. Meisner, *Phys. Rev. B* 59, 8615 (1999).
10. W. Xie, A. Weidenkaff, X. Tang, Q. Zhang, J. Poon, T.M. Tritt, *Nanomaterials* 2, 379 (2012).
11. C.G. Fu, H.H. Xie, Y.T. Liu, T.J. Zhu, J. Xie, X.B. Zhao, *Intermetallics* 32, 39 (2013).
12. P. Qiu, J. Yang, X. Huang, X. Chen, L. Chen, *Appl. Phys. Lett.* 96, 152105 (2010).
13. G.K.H. Madsen, *J. Am. Chem. Soc.* 128, 12140 (2006).
14. G. Ding, G.Y. Gao, L. Yu, Y. Ni, K. Yao, *J. Appl. Phys.* 119, 025105 (2016).
15. J.M. Mena, H.G. Schoberth, T. Gruhn, H. Emmerich, *J. Alloys Compd.* 650, 728 (2015).
16. J. Yang, Z.G. Mei, L. Xi, W. Zhang, and L.D. Chen, in *Proceedings of International Symposium on EcoTopia Science ISETS'07* 52 (2007).
17. Y. Benallou, K. Amara, B. Doumi, O. Arbouche, M. Zemouli, B. Bekki, A. Mokaddem, *J. Comput. Electron.* 16, 1 (2016).
18. G. Wang, D. Wang, *J. Alloys Compd.* 682, 375 (2016).
19. K. Manoj, B. Sanyal, *J. Alloys Compd.* 622, 388 (2015).
20. G. Ding, G.Y. Gao, K.L. Yao, *J. Phys. D Appl. Phys.* 47, 385305 (2014).

21. J. Oestreich and U. Probst, in *Twenty-First International Conference on Thermoelectrics Proceedings ICT'02* 135 (2002).
22. F. Kong, Y. Hu, H. Hou, Y. Liu, B. Wang, L. Wang, *J. Solid State Chem.* 196, 511 (2012).
23. M. Onoue, F. Ishii, T. Oguchi, *J. Phys. Soc. Jpn.* 77, 054706 (2008).
24. K. Benchrif, A. Yakoubi, O.M. Della, M. Abid, H. Khachai, R. Ahmed, R. Khenata, S. Bin-Omran, S.K. Gupta, G. Murttaza, *J. Electron. Mater.* 45, 3479 (2016).
25. O.M. Abid, S. Menouer, A. Yakoubi, H. Khachai, S. Bin Omran, G. Murtaza, D. Prakash, R. Khenata, K.D. Verma, *Superlattices Microstruct.* 93, 171 (2016).
26. T. Djaafri, A. Djaafri, A. Elias, G. Murtaza, R. Khenata, R. Ahmed, S. Bin Omran, D. Rached, *Chin. Phys. B* 23, 087103 (2014).
27. X. Li, C. Xia, M. Wang, Y. Wu, D. Chen, *Metals* 7, 317 (2017).
28. J. Wallenius, D. Westlén, *Ann. Nucl. Energy* 35, 60 (2008).
29. C. Herranz-Diez, C. Mas-Moruno, S. Neubauer, H. Kessler, F.J. Gil, M. Pegueroles, *ACS Appl. Mater.* 8, 2517 (2016).
30. O. Levy, G.L.W. Hart, S. Curtarolo, *Acta Mater.* 58, 2887 (2010).
31. S. Chibani, O. Arbouche, K. Amara, M. Zemouli, Y. Benallou, Y. Azzaz, B. Belgoumène, M. Elkeurti, M. Ameri, *J. Comput. Electron.* 16, 765 (2017).
32. R. Gautier, X. Zhang, L. Hu, L. Yu, Y. Lin, T.O.L. Sunde, D. Chon, K.R.A. Poeppelmeier, A. Zunger, *Nat. Chem.* 7, 308 (2015).
33. G. Wang, J.H. Wei, *Comput. Mater. Sci.* 124, 311 (2016).
34. Z.-G. Song, C. Felser, Y. Sun, *Phys. Rev. B* 98, 165131 (2018).
35. G.Y. Yonggang, X. Zhang, A. Zunger, *Phys. Rev. B* 95, 085201 (2017).
36. M.S. Lee, F.P. Poudeu, S.D. Mahanti, *Phys. Rev. B* 83, 085204 (2011).
37. https://www.quantum-espresso.org/. Accessed 20 June 2019.
38. P. Giannozzi, S. Baroni, N. Bonini, M. Calandra, R. Car, C. Cavazzoni, D. Ceresoli, G.L. Chiarotti, M. Cococcioni, I. Dabo, A. Dal Corso, S. de Gironcoli, S. Fabris, G. Fratesi, R. Gebauer, U. Gerstmann, C. Gougoussis, A. Kokalj, M. Lazzeri, L. Martin-Samos, N. Marzari, F. Mauri, R. Mazzarello, S. Paolini, A. Pasquarello, L. Paulatto, C. Sbraccia, S. Scandolo, G. Sclauzero, A.P. Seitsonen, A. Smogunov, P. Umari, R.M. Wentzcovitch, *J. Condens. Mater. Phys.* 21, 395502 (2009).
39. P. Perdew, K. Burke, M. Ernzerhof, *Phys. Rev. Lett.* 77, 3865 (1996).
40. M. Methfessel, A.T. Paxton, *Phys. Rev. B* 40, 3616 (1989).
41. S. Baroni, P. Giannozzi, A. Testa, *Phys. Rev. Lett.* 58(18), 1861 (1987).
42. S. Baroni, S. De Gironcoli, A. Dal Corso, P. Giannozzi, *Rev. Mod. Phys.* 73, 515 (2001).
43. M.J. Mehl, *Phys. Rev. B* 47, 2493 (1993).
44. M.J. Mehl, J.E. Osburn, D.A. Papaconstantopoulos, B.M. Klein, *Phys. Rev. B* 41, 10311 (1990).
45. G.D. Yıldız, Y.G. Yıldız, S. Al, A. İyigör, N. Arıkan, *Int. J. Mod. Phys. B* 32, 1850214 (2018).
46. S. Al, N. Arikan, S. Demir, A. Iyigör, *Phys. B Condens. Matter.* 16, 531 (2018).
47. R.P. Singh, *J. Magn. Alloy* 2, 349 (2014).
48. M. Born, K. Huang, M. Lax, *Am. J. Phys.* 23, 474 (1955).
49. R. Ravindran, L. Fast, P.A. Korzhavyi, B. Johansson, J. Wills, O. Eriksson, *J. Appl. Phys.* 84, 4891 (1998).
50. D.H. Chung, W.R. Buessem, in *Anisotropy in Single Crystal Refractory Compound*, ed. by F.W. Vahldiek, A. Mersol (Plenum, New York, 1968).
51. D.G. Pettifor, *Mater. Sci. Tech. Lond.* 8, 345 (1992).
52. S.F. Pugh, *Philos. Mag.* 45, 823 (1954).
53. S. Chadov, X. Qi, J. Kübler, G.E. Fecher, C. Felser, S.C. Zhang, *Nat. Mater.* 9, 541 (2010).
54. A.T. Petit, P.L. Dulong, *Ann. Chim. Phys.* 10, 395 (1819).

Publisher's Note Springer Nature remains neutral with regard to jurisdictional claims in published maps and institutional affiliations.